water

MDPI

Article

Potential Impacts of Future Climate Change Scenarios on Ground Subsidence

Antonio-Juan Collados-Lara [1,*], David Pulido-Velazquez [1], Rosa María Mateos [2] and Pablo Ezquerro [3]

1 Department of Research on Geological Resources, Geological Survey of Spain (IGME), Urb. Alcázar del Genil, 4-Edif. Bajo, 18006 Granada, Spain; d.pulido@igme.es
2 Geohazard InSAR Laboratory and Modelling Group, Geological Survey of Spain (IGME), Urb. Alcázar del Genil, 4-Edif. Bajo, 18006 Granada, Spain; rm.mateos@igme.es
3 Geohazard InSAR Laboratory and Modelling Group, Geological Survey of Spain (IGME), Ríos Rosas, 23, 28003 Madrid, Spain; p.ezquerro@igme.es
* Correspondence: ajcollados@gmail.com

Received: 12 December 2019; Accepted: 8 January 2020; Published: 13 January 2020

check for updates

Abstract: In this work, we developed a new method to assess the impact of climate change (CC) scenarios on land subsidence related to groundwater level depletion in detrital aquifers. The main goal of this work was to propose a parsimonious approach that could be applied for any case study. We also evaluated the methodology in a case study, the Vega de Granada aquifer (southern Spain). Historical subsidence rates were estimated using remote sensing techniques (differential interferometric synthetic aperture radar, DInSAR). Local CC scenarios were generated by applying a bias correction approach. An equifeasible ensemble of the generated projections from different climatic models was also proposed. A simple water balance approach was applied to assess CC impacts on lumped global drawdowns due to future potential rainfall recharge and pumping. CC impacts were propagated to drawdowns within piezometers by applying the global delta change observed with the lumped assessment. Regression models were employed to estimate the impacts of these drawdowns in terms of land subsidence, as well as to analyze the influence of the fine-grained material in the aquifer. The results showed that a more linear behavior was observed for the cases with lower percentage of fine-grained material. The mean increase of the maximum subsidence rates in the considered wells for the future horizon (2016–2045) and the Representative Concentration Pathway (RCP) scenario 8.5 was 54%. The main advantage of the proposed method is its applicability in cases with limited information. It is also appropriate for the study of wide areas to identify potential hot spots where more exhaustive analyses should be performed. The method will allow sustainable adaptation strategies in vulnerable areas during drought-critical periods to be assessed.

Keywords: ground subsidence; climate change; Vega de Granada aquifer

1. Introduction

In many agricultural regions, as well as areas with a rapid urbanization and population growth, prolonged groundwater exploitation due to increasing water demand is causing land subsidence impacts [1–7]. In many coastal and delta cities, such as Ho Chi Minh, Bangkok, Manila, Tokyo, and Jakarta, land subsidence considerably exceeds (by up to 10 times) absolute sea level rise, which increases flood vulnerability and triggers severe, damaging impacts [8]. Sinking cities—within the framework of global change—is and will be a transnational threat.

Land subsidence is related to falling groundwater levels in (generally) unconsolidated alluvial or basin-fill aquifers with a significant proportion of compressible fine-grained materials. Increases in effective stresses—caused by headwater declines—determine the aquifer system compaction at local or regional scales [9]. This deformation is typically elastic (reversible) and results in small vertical displacements, but when the aquifer is subjected to head declines that exceed the critical levels, much of the compaction is related to an inelastic deformation and the accompanying subsidence is permanent [10].

Differential interferometric synthetic aperture radar (DInSAR) techniques are satellite-based remote-sensing tools that have been applied successfully for monitoring land subsidence thanks to their high spatial and temporal coverage, fast data acquisition, and low cost [11]. They are capable of measuring mm-scale ground displacements at a spatial resolution of 5–10 m over large regions (hundreds to thousands of square kilometers). They have been widely applied in numerous recent studies of land subsidence triggered by intense groundwater withdrawals [12–15]. A prominent case is Jakarta, the capital city of Indonesia (around 10 million people), where subsidence values of 28 cm/year have been registered in some locations. The impacts in Jakarta have been seen in several forms: not only cracking and damage in buildings and infrastructure, but subsidence also enlarges the (tidal) flooding inundation areas and makes the coast more vulnerable to sea-level-rise phenomena [1]. Indonesian authorities think the capital should be relocated.

In the present work, we applied the persistent scatterer interferometry technique (PSInSAR), an operational tool for precise ground deformation mapping, acting as a geodetic network [16]. This technique allows quantification of deformation measurements, combining them with geological and hydrogeological data in a geographical information system (GIS). The application of PSInSAR has improved rapidly in the last decade, and it is now a valuable tool for monitoring seasonal and long-term aquifer-system responses to groundwater pumping.

In the literature, we found many different approaches that have been employed to model the impact of groundwater level depletion on the subsidence. Some of them are based on physically based distributed hydro-geomechanical models [17,18], but we also found other approaches such as machine learning [19] and conceptual [20] or simple regression approaches [21], like the one that was employed in this work.

In order to assess potential future impacts of climate change (CC) in a rational way, we need to use the climatic scenarios generated by simulating with climatic models the emission scenarios identified by the Intergovernmental Panel of Climate Change (IPCC). The most recent of these are those included in the 5th assessment report [22], the RCP scenarios. These scenarios are not predictions of future climate; they are internally consistent pictures of plausible future climates that constitute a basis for other workers to evaluate the possible impacts of CC [23]. In order to make this information relevant to assessment of impacts in specific case studies, they have to be translated to regional and local scales by applying statistical correction techniques that take into account historical data [24].

Despite the spread of uncertainties involved in the assessment of future CC impacts, there is no excuse for delays or inaction in assessing/identifying adaptation strategies, taking into account that there are environments that could be very vulnerable [25]. The market for technologies for adaptation to CC is growing rapidly, given that "the cost of repairing damages is estimated to be six times greater than adaptation costs" (H2020WATER-2014/2015). In the literature, we found multiple examples of the propagation of future CC scenarios in order to assess hydrological impacts at different scales, including continental [26,27], country [28,29], river basin [30,31], and aquifer [28,32] systems. Nevertheless, the literature on the assessment of the potential future impacts of CC on land subsidence is very limited [33]. Only a few works have been developed on identification and assessment of potential adaptation strategies, like the work published by Brouns et al. [34], in which a bottom-up approach was applied to define the scenarios.

The main objective of this research was to propose a new, parsimonious approach [35,36] with which to perform a first assessment of potential CC impacts on land subsidence related to groundwater-level depletion in detrital aquifers. We also applied and validated it in the Vega de Granada aquifer (southern Spain). We have proposed a general approach applicable to any type of aquifer including in coastal areas, which are more vulnerable to subsidence [37,38]. The main innovative aspect of the proposed methodology is its applicability in cases with limited information through a combination of several parsimonious techniques: (1) a statistical approach for CC generation, (2) a simple hydrological approach to assess the impacts of CC on groundwater levels, and (3) simple linear regression models to propagate the impacts to land subsidence. The model might be also useful for a preliminary assessment of different adaptation strategies. It does not require a distributed groundwater flow model of the system [39,40]. Taking into account the uncertainties around future potential CC scenarios, the model provides a useful first approach, even in wide areas (e.g., country or continental scale), that can identify potential hot spots where more exhaustive analyses should be performed.

2. Case Study

The Vega de Granada is a flat region located in the metropolitan area of the city of Granada (southern Spain, 530,000 people) (see Figure 1). With an extension of 200 km^2, the Vega de Granada is a traditional agricultural region with increasing urban growth during recent decades. Both agricultural and urban demands exert a high pressure on the aquifer. The river Genil flows (from SE to NW) through the center of the basin, being the aquifer's main drainage axis [41].

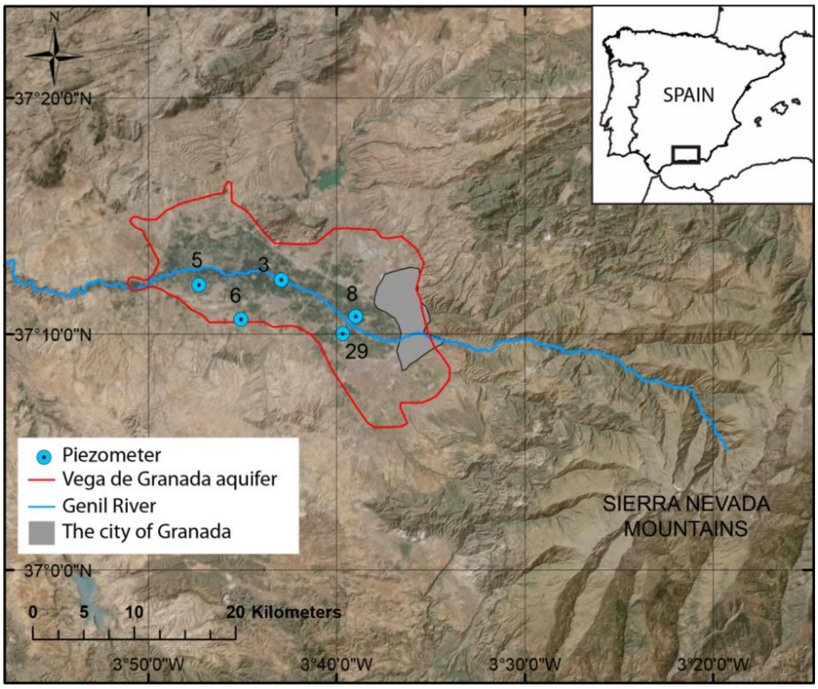

Figure 1. Location of the case study. The Vega de Granada aquifer is of regional importance. It is located within the Granada Basin domain (southern Spain) and in the central sector of the Betic cordillera (Sierra Nevada).

From the geological point of view, the Vega de Granada is within the Granada Basin domain, in the central sector of the Betic cordillera. It is a tectonic depression delineated by normal faults which control the basin infill. The Vega de Granada detrital aquifer presents a multilayer and heterogeneous structure with quaternary levels of gravel, sand, silt, and clay, with a maximum thickness of 250 m in its central part [15,42,43]. Both the river sedimentation and the surroundings alluvial fans (related to the normal faults) determine the facies distribution.

The Vega de Granada aquifer is of regional importance. With renewable water resources of about 160 hm^3/yr [43], groundwater exploitation has intensified considerably in recent decades because of urban sprawl, particularly during the severe droughts that periodically affect the region.

The heterogeneous sedimentary structure controls the great spatial variability of the hydraulic parameters in the aquifer (permeability, transmissivity, etc.) and the distribution of the most productive wells. All these variables in the aquifer can be used to explain its spatial and temporal response to hydraulic head changes and the subsequent vertical ground movements.

3. Data and Methods

A flowchart of the proposed method has been represented in Figure 2.

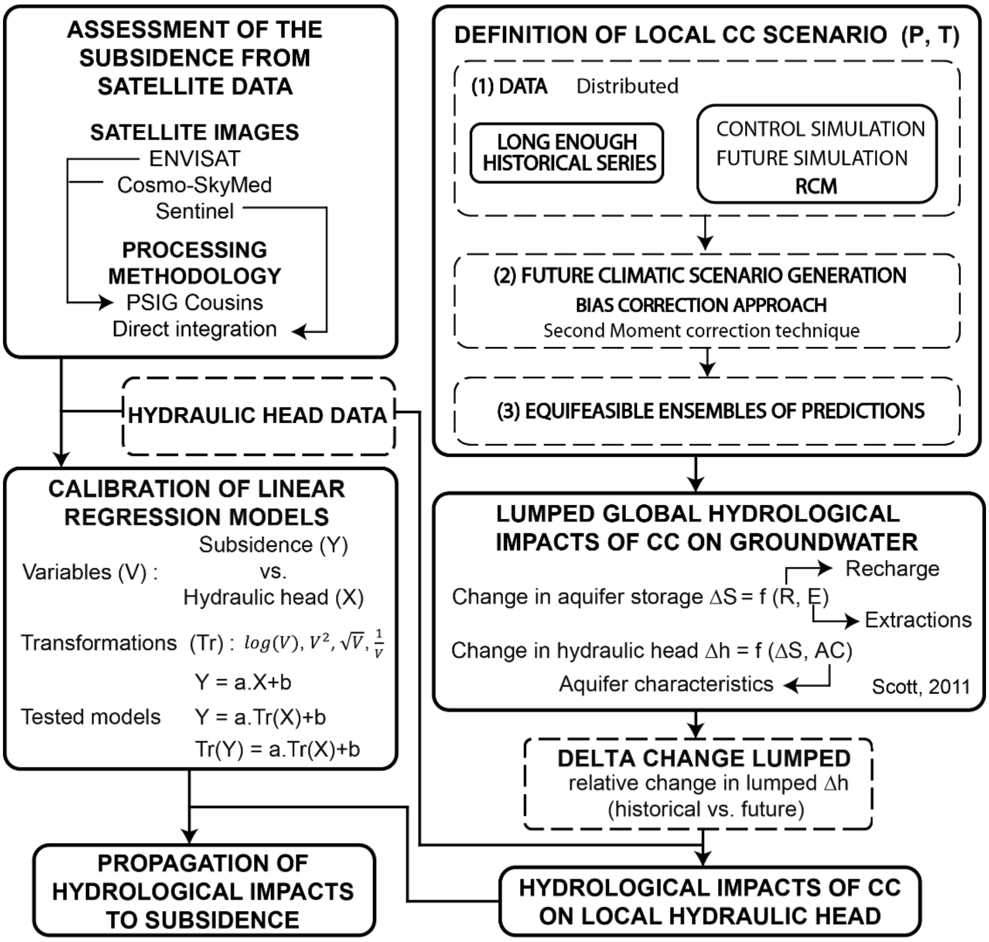

Figure 2. Flow chart of the proposed methodology.

3.1. Data Employed and Their Origins

The historical climate data for our case study were taken from Version 04 of the Spain02 dataset [44] (see Figure 3a,b). The Spain02 dataset includes daily temperature and precipitation estimates from observations (around 2500 quality-control stations) of the Spanish Meteorological Agency.

We also used data from individual global future climate projections (see Table 1) produced by regional climate models (RCM) nested within different global circulation models (GCM). This information was retrieved from the Coordinated Regional Downscaling Experiment (CORDEX) project [45]. The Spain02 project uses the same grids as the EURO-CORDEX project, which has a spatial resolution of approximately 12.5 km.

In addition, we also employed some hydrological information, including hydraulic head evolution in different piezometers obtained from the Spanish official network for monitoring the quantitative state of groundwater (see their location in Figure 1) and the historical recharge and pumping rates within the aquifer, which were taken from the information included in the Guadalquivir River Basin Plan (2015–2021).

Table 1. Regional climate models (RCMs) and global circulation models (GCMs) considered.

GCM / RCM	CNRM-CM5	EC-EARTH	MPI-ESM-LR	IPSL-CM5A-MR
CCLM4-8-17	×	×	×	
RCA4	×	×	×	
HIRHAM5		×		
RACMO22E		×		
WRF331F				×

For those wells, we also used information about the land subsidence rates obtained by applying PInSAR techniques. The average vertical displacement based on the time series was estimated by using buffer areas with a radius of 1000 m for each piezometer and considering all PSI (persistent scatterer interferometry) data included in the area [15]. The percentage of fine-grained material (clay and silt) for each piezometer was obtained by exploiting geological data recorded in 38 boreholes drilled in the area. They were interpreted [15] to provide isolines of fine-grained sediment percentage, taking into account the clay and silt content in the first 50 m of the borehole, as the borehole depths were quite variable (from 50 to 122 m).

The results showed higher clay content in the piezometers located in the northern and southern extremes of the aquifer, as well as in its central part (see Table 2).

Table 2. Content of clay and silt in the considered piezometers.

Piezometer	Clay and Silt Content (%)
5	40
3	5
6	70
8	20
29	20

The historical data and the future trends of population within the area were obtained from the Spanish Statistical Office <https://www.ine.es/>.

3.2. Assessment of Subsidence from Satellite Data

In the present study, spatial and temporal ground surface deformation assessment was conducted by exploiting 70 SAR images from three different satellites: ENVISAT (2003–2009, C band), Cosmo-SkyMed (2011–2014, X band), and Sentinel 1A (2015–2016, C band). The processing methodologies applied for each dataset were: (1) PSIG Cousins [46] for the ENVISAT and COSMO-Sky-Med datasets, and (2) direct integration approach [47] for the Sentinel 1A dataset. More detailed specifications can be found in Mateos et al. [15]. This combination allowed a thorough assessment of the ground deformation pattern in the aquifer and both the temporal and spatial dimensions of the subsidence.

PSInSAR measurements were obtained in the aquifer of the Vega de Granada (southern Spain), covering a large temporal span of 13 years (from 2003 to 2016). In this time, a severe drought affected the area during the ENVISAT period (2003–2006), and greater groundwater withdrawals took place.

PSInSAR data were correlated (temporally and spatially) with hydraulic head changes in the aquifer along the monitoring period, and with geological data (from boreholes) regarding the clay and silt content in the aquifer. Based on the borehole information, isolines of fine sediments percentage were obtained by Mateos et al. [15]. Clay and silt content is key information which can explain the spatial response of and aquifer system to hydraulic head changes and the subsequent vertical land movements.

3.3. Definition of Local CC Scenarios

A statistical method was used to define local future global change scenarios for the pilot, based on the historical information for the adopted reference period (1986–2015) and the available RCM simulations.

These scenarios were derived from RCM simulations available in the CORDEX project [45] for the most pessimistic emission scenario, RCP 8.5, and the temporal horizon 2016–2045. The future series were generated by applying the first- and second-moment correction technique under the bias-correction approach [24]. The bias-correction techniques applied a perturbation (transformation function) to the control series of the RCM simulations to obtain another series with statistics more similar to the historical series. The transformation function in the first- and second-moment correction technique is defined by focusing on the mean and standard deviation of the climate series. The same transformation function was applied to the future simulations of the RCM to obtain the climate change projections. An equifeasible ensemble of the individual climate change projections have been proposed in order to define more robust climate projections that are more representative than those based on a single model [32,48].

3.4. Hydrological Impacts of Climate Change on Groundwater Levels

A simple approach proposed by Scott [49] was applied to assess future CC impacts on global lumped drawdowns due to the future potential rainfall recharge and pumping. Following this approach, simple balance equations were applied in order to assess the global lumped change in hydraulic head (Δh_t) from aquifer storage (ΔS_t), which was calculated as follows.

$$\Delta S_t = R_t - E_t \tag{1}$$

where R_t is the aquifer rainfall recharge and E_t is the aquifer extraction, which can be obtained from Equation (2).

$$E_t = Eag_t - Enonag_t \tag{2}$$

where Eag_t represents the agricultural extractions and $Enonag_t$ the non-agricultural extractions. They were calculated using Equations (3) and (4), respectively.

$$Eag_t = Eag_{t-1}\left[1 + \frac{ET_t - ET_{t-1}}{ET_{t-1}}\right] \tag{3}$$

$$Enonag_t = Enonag_{t-1}\left[1 + \frac{Pop_t - Pop_{t-1}}{Pop_{t-1}}\right] \tag{4}$$

where ET is the evapotranspiration calculated using the Blaney–Criddle method ($ET = p(0.46\text{Tmean} + 8)$) on the basis of monthly temperature in °C (Tmean) and latitude-derived sunshine-hour fraction (p), and Pop is the population of the area.

Finally, the hydraulic head (Δh_t) was calculated using Equation (5).

$$\Delta h_t = \frac{\Delta S_t}{A \times S_y} \tag{5}$$

where A is the aquifer area and S_y the specific yield.

The initial conditions used to simulate the recharge (R_{t-1}) and pumping (agricultural or non-agricultural, Eag_{t-1} and $Enonag_{t-1}$) evolutions were taken from the information included in the Guadalquivir River Basin Plan (2015–2021).

The lumped approach proposed by Scott [49] was also applied to estimate the lumped hydraulic head drawdowns in the reference historical period (1986–2015). The method allowed estimation of the delta change (percentage increase) in the lumped aquifer drawdowns, taking into account the relative difference between the maximum lumped drawdowns in the historical and the future periods (2016–2045). These results were obtained under the assumption that a business-as-usual management scenario will be maintained in the future. The future potential hydraulic head in each piezometer was obtained by applying a delta change correction, using the lumped change to modify the historical evolution (for the reference period) of this variable within the piezometer.

3.5. Propagation of Hydrological Impacts to Subsidence

Simple linear regression models have been defined in order to approximate subsidence as a function of hydraulic head drawdowns in the selected head observation wells. We tested different transformations (Tr(X)) of the explanatory and target variables (logarithm, inverse, square, and square-root mathematical transformations) in order to identify the one that provided the best approximation to the empirical data for this problem (see Table 3).

The models used assume that there is a linear relation between both variables, the dependent variable and the explanatory variable and its transformations, which is reasonable if the deformation is elastic. An analysis of the linear correlation depending on the percentage of clay and silt content in the ground was also proposed in order to identify and discuss when linear regression might represent a better approach.

Table 3. Regression models and transformation of variables applied. The symbol * represents the tested combinations of models and transformation of variables.

	Tr(X)				
Model	**-**	**X^2**	**sqrt(X)**	**log(X)**	**1/X**
$Y = a \times X + b$	*	-	-	-	-
$Y = a \times Tr(X) + b$	-	*	*	*	*
$Tr(Y) = a \times Tr(X) + b$	-	*	*	*	*

4. Results and Discussion

For the case study, the future equifeasible ensemble series obtained by applying the bias correction approach showed a mean global temperature increase of 7.72% and a mean global reduction of precipitation of 6.24%. Figure 3 shows the mean historical and future yearly series of precipitation and temperature.

The hydrological approach described in Section 3.4 was employed to propagate the generated future local climatic series to assess future hydrological impacts in terms of future recharge and pumping (Figure 4).

The mean reduction of the recharge and increase of pumping expected for the potential future horizon contemplated were 1.4 $Hm^3\ year^{-1}$ and 1 $Hm^3\ year^{-1}$, respectively. In the global budget, the impacts of CC on the recharge will have a higher influence on the future hydraulic head drawdowns.

Taking into account the projected changes in the future recharge and withdrawals within the aquifer, the global lumped hydraulic head drawdowns were obtained by applying the Scott [49] approach. The maximum lumped drawdown obtained in the future was 3.3% greater than the one obtained in the historical period. This relative change was employed to apply a delta change to correct the historical drawdowns in the selected head-observation wells (see Figure 1), obtaining for the future period the values presented in Figure 9.

In order to propagate the impacts of these hydraulic head drawdowns on the subsidence, different regression approaches were tested (see Figure 2). In each piezometer, the coefficient of determination of the calibrated models depended on the selected transformation (see results for the tested models in Figure 5). The two best combinations of model and transformation were $S = a \times P + b$ and $S^2 = a \times P^2 + b$, where S represents the subsidence and P the hydraulic head (Models A and F in Figure 5). The mean R^2 values of these models for the five considered piezometers were 0.60 and 0.73, respectively. These models were employed to predict the impacts of the potential future CC scenario on subsidence. An example of the fit of the regression models for the target variable (subsidence) and the explanatory variable (hydraulic head) is included in Figure 6 for Piezometer 3 and the selected models.

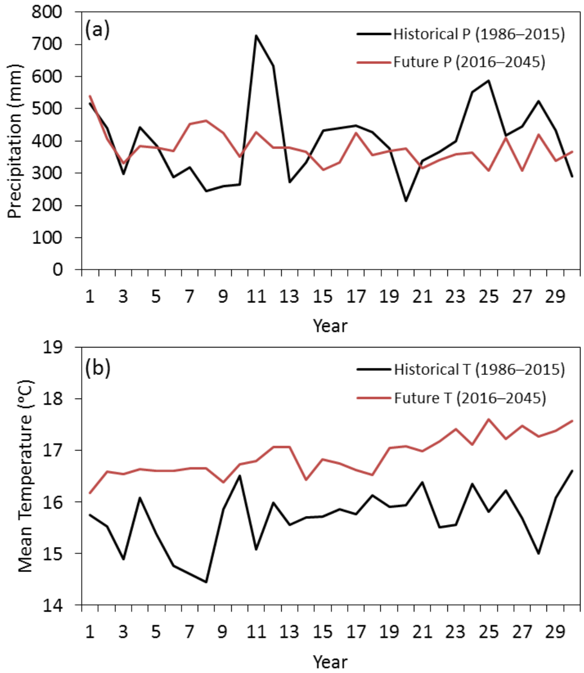

Figure 3. Yearly mean historical and generated future series of precipitation (**a**) and mean temperature (**b**) for the periods 1986–2015 and 2016–2045. The historical data were obtained from the Spain02 dataset and the future series was generated by applying the proposed methodology.

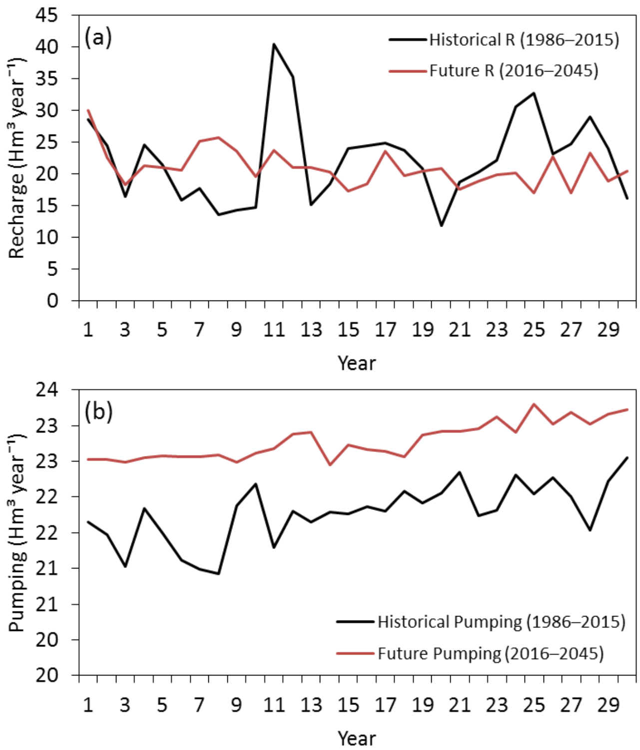

Figure 4. Yearly mean historical and future series of recharge (**a**) and withdrawals (**b**) for the mean year in the periods 1986–2015 and 2016–2045. The historical data were obtained using the methodology proposed by Scott [49] and historical recharge and pumping rates from the Guadalquivir River Basin Plan (2015–2021). The future series were generated by applying the proposed methodology.

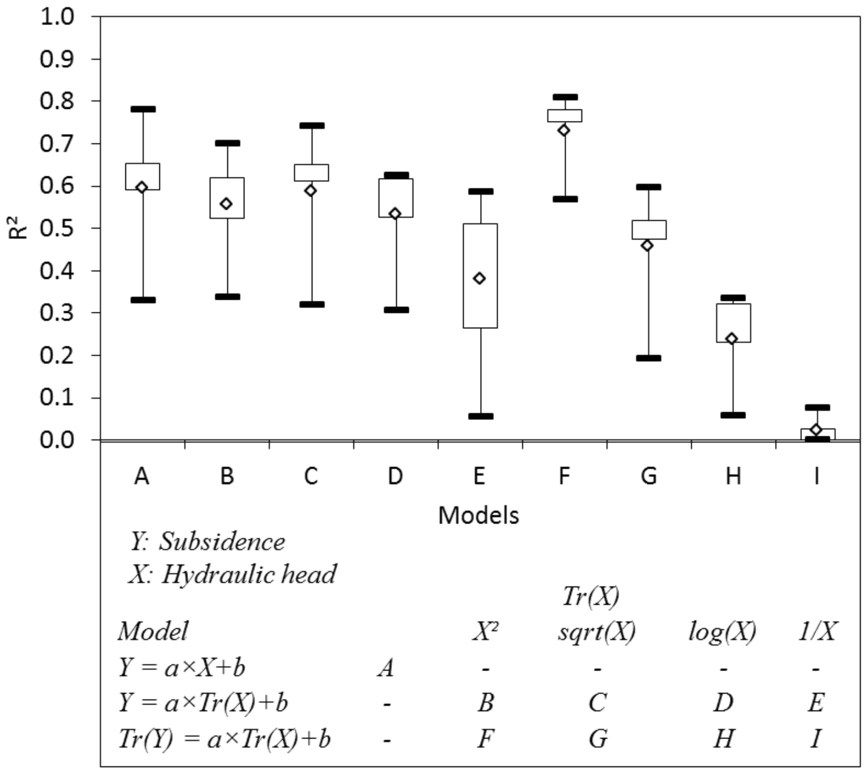

Figure 5. Coefficient of determination (R^2) of the tested models for the five considered piezometers.

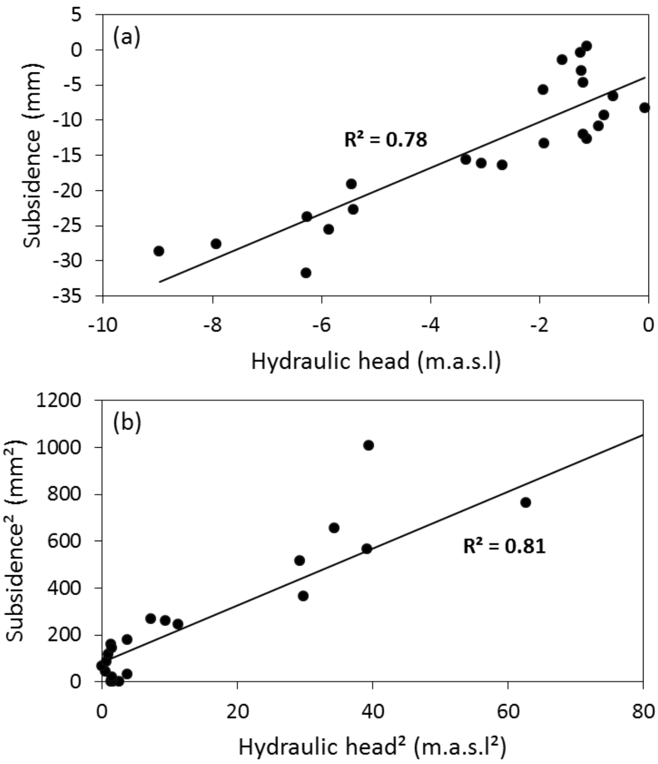

Figure 6. Relationship between the target variable and the explanatory variable for the two best linear regression models (S = a × P + b; $S^2 = a \times P^2 + b$) for Piezometer 3.

The selected models were compared in terms of mean error and mean squared error too (see Figure 7). The two models showed a mean error of 0.0 mm; the model S = a × P + b showed a mean squared error of 20.63 mm^2 and the model $S^2 = a \times P^2 + b$ showed a mean squared error of 23.44 mm^2.

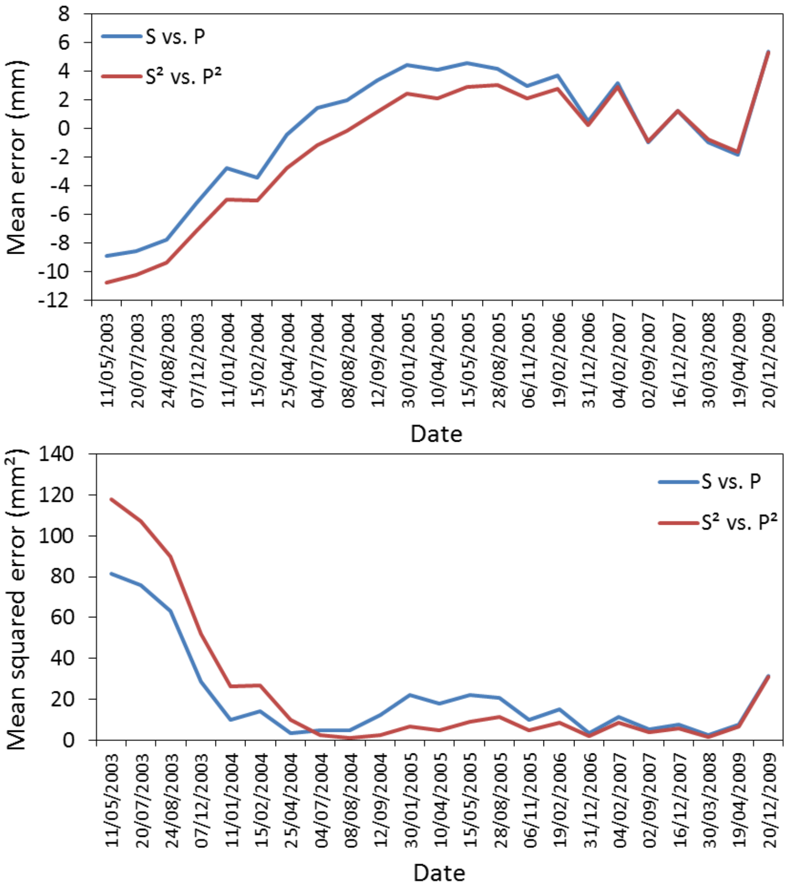

Figure 7. Mean values of the mean error and mean squared error for the five considered piezometers, obtained for the two best linear regression models (S = a × P + b; $S^2 = a \times P^2 + b$).

The granulometry of subsurface sediments has a significant impact on the ground subsidence. We analyzed the influence of the percentage of clay and silt (in the surrounding area of the piezometer) on the historical subsidence rate and the linear behavior of the subsidence, assessed in terms of the R^2 of the regression models.

Figure 8a shows the relationship between the percentage of fine-grained material and the historical subsidence rate, and Figure 8b the coefficient of determination obtained for the best approach for each piezometer vs. the percentage of clay and silt. In general, a higher percentage of fine-grained material was related to a lower subsidence rate, but the correlation of this relationship was poor (R^2 = 0.24). On the other hand, higher coefficients of determination were related with a more linear behavior, which was observed for the cases with lower percentage of clay and silt. Note that in general, the relationship between the percentage of fine-grained material and the coefficients of determination of the linear models had a good correlation (R^2 higher than 0.8). In fact, PSInSAR results showed an inelastic deformation in the aquifer where a higher clay–silt content was identified [15]. Percentage of fine-grained material, thickness, and distribution of lenses significantly affected spatiotemporal subsidence patterns, which was in agreement with the results observed by other authors [10,50].

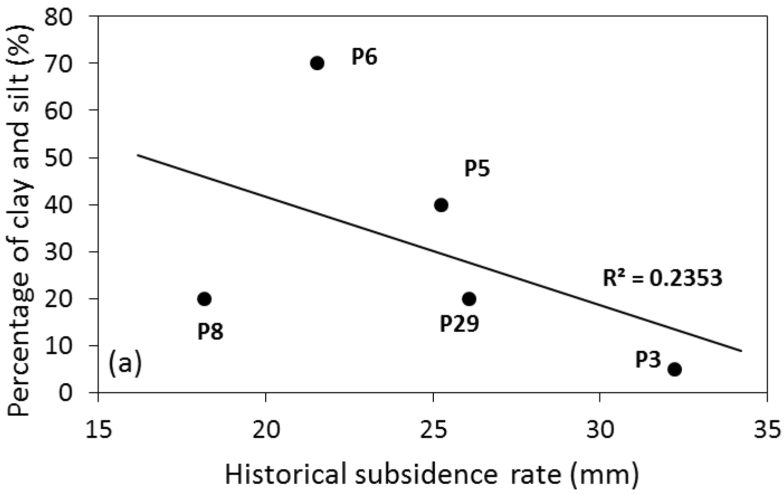

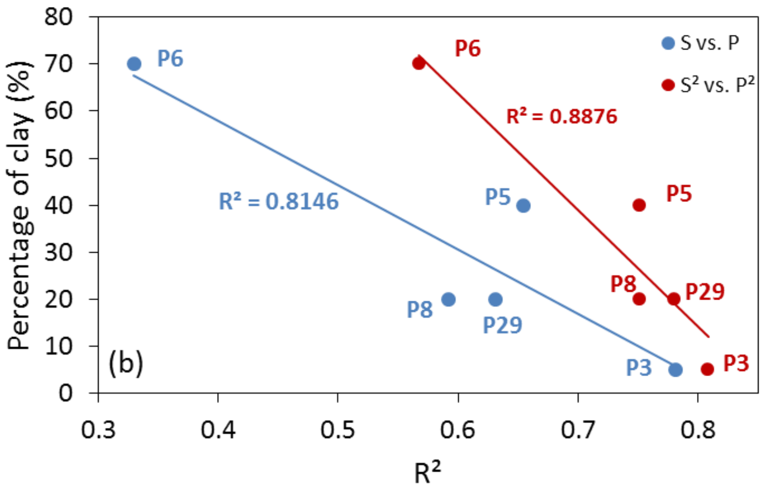

Figure 8. Relationship between the percentage of clay and silt and the historical subsidence rate (**a**) and the correlation coefficients obtained for the two best linear regression models ($S = a \times P + b$; $S^2 = a \times P^2 + b$) (**b**).

For Piezometer 6, which was the one with highest percentage of clay (70%), we obtained very low coefficient of determination (0.33 and 0.57 for the models $S = a \times P + b$ and $S^2 = a \times P^2 + b$, respectively) and the linear regression approach was not appropriate. For this reason, we have not included the results for the assessment of the future subsidence for this observation well.

The propagation of the impacts of the potential future CC scenario on subsidence (Figure 9) showed important increases of the maximum subsidence (55.3% and 52.7% for the models $S = a \times P + b$ and $S^2 = a \times P^2 + b$, respectively) with respect to the historical maximum observed values. The highest increase of the maximum subsidence (68.3% and 65.7% for the models $S = a \times P + b$ and $S^2 = a \times P^2 + b$, respectively) with respect to the historical maximum observed values occurred in Piezometer 5, which was located in the western area where the percentage of clay was 40%.

In terms of mean subsidence (see Figure 10) the mean increase of subsidence was 4.1 mm and 4.5 mm for the models $S = a \times P + b$ and $S^2 = a \times P^2 + b$, respectively. The piezometer with the highest increase of mean subsidence was Piezometer 3, with 5.4 mm and 5.9 mm for the models $S = a \times P + b$ and $S^2 = a \times P^2 + b$, respectively. This piezometer showed the highest variability of subsidence in the historical and future periods, and had the lowest content of clay and silt.

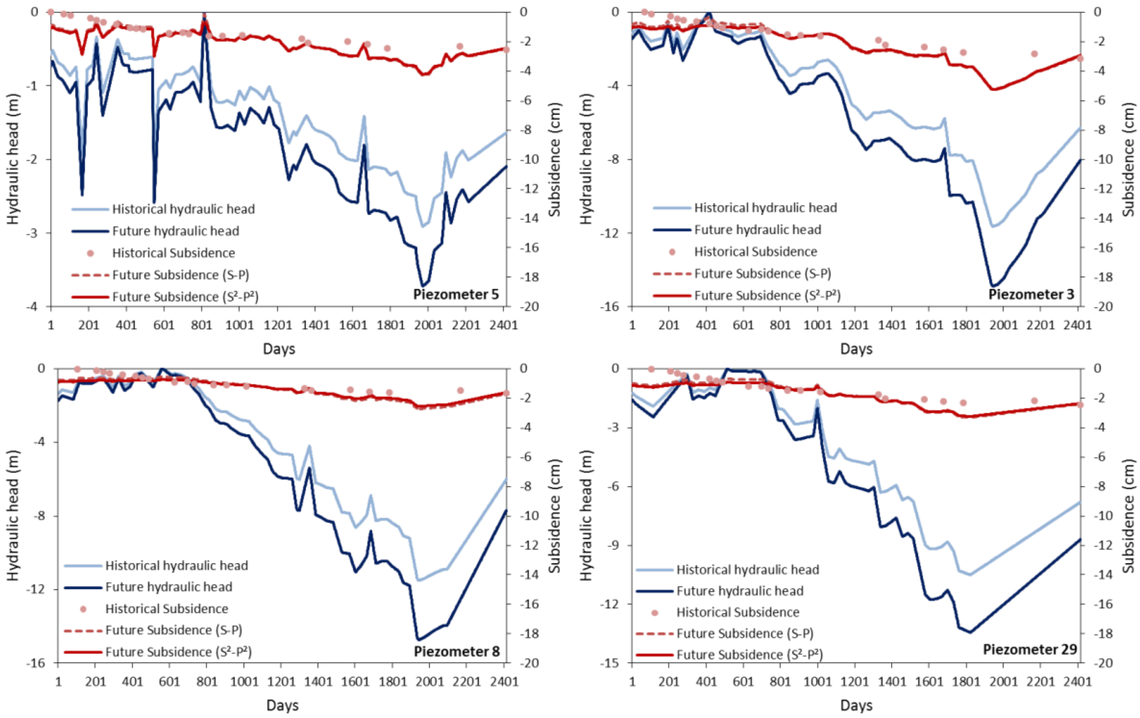

Figure 9. Historical and future subsidence and hydraulic head for the two best linear regression models (S = a × P + b; S^2 = a × P^2 + b).

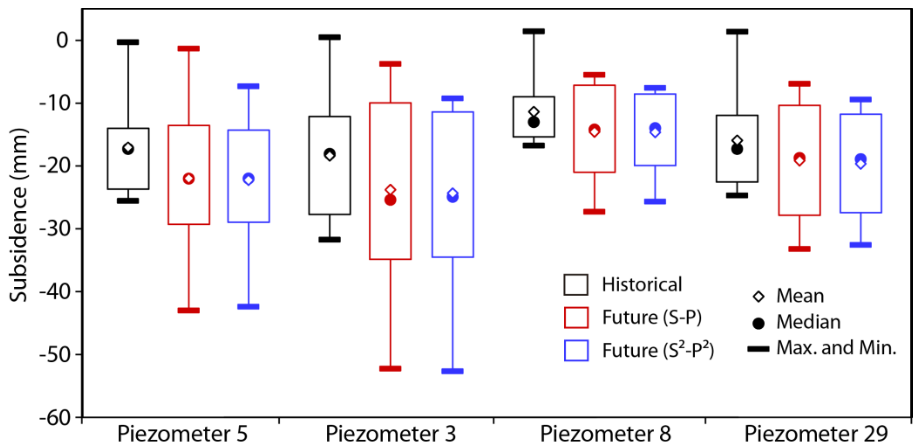

Figure 10. Historical and future subsidence for the two best linear regression models (S = a × P + b; S^2 = a × P^2 + b).

Hypotheses Assumed and Limitations

The assessment performed assumed some hypotheses or made simplifications as follows.

Climate change scenarios

- We generated future local climatic scenarios only for the horizon 2016–2045, assuming the most pessimistic emissions scenario (RCP 8.5) and applying a simple statistical correction (first- and second-moment correction) to correct the observed biases.
- An equifeasible ensemble of the potential future local climate scenarios was proposed to define a more representative scenarios by combining projections of different climatic models.

Propagation of climate change in terms of hydrological impacts

- A simple approach proposed by Scott [49] was applied in order to perform the assessment of future CC impacts on global lumped drawdowns. It has the advantages that it does not require the use of a previously calibrated distributed model, and can be applied in cases with limited information. A delta change approach defined from this lumped variable was employed to assess drawdowns in the piezometers by correcting the historical series. More precise results could be obtained in cases where a physically distributed model is directly used to propagate climate change impacts.
- This work focused exclusively on the impacts produced by the reduction in rainfall recharge and the increase of pumping due to potential future local climate scenarios and changes in population.
- We assumed a business-as-usual management scenario to assess the impacts of future potential local climate scenarios on subsidence. Other management scenarios could be considered in order to assess the benefit of potential adaptation strategies.

Propagation of hydrological impacts to subsidence

- We assumed a linear relationship between the hydraulic head drawdowns and the subsidence in the piezometers. This allowed us to use a simple regression model. We also assumed that the model was valid in the range in which the future assessment was performed.

5. Conclusions

A method to assess impact of potential future CC scenarios on land subsidence related to groundwater level depletion in detrital aquifers was described and applied in a case study. It does not require a previous distributed groundwater flow model of the aquifer, which is an important advantage for its applicability in cases with limited information. Taking into account the uncertainties around future potential CC scenarios, it could provide a useful first assessment of its impacts on subsidence. It allows analyses of wide areas to be performed in order to identify potential hot spots that require more exhaustive analysis. It will help to assess sustainable adaptation strategies in identified vulnerable areas, taking into account subsidence issues during drought-critical periods. The methodology was applied in the Vega de Granada aquifer (Granada, SE Spain). Good correlation between groundwater level depletion and the subsidence was obtained in the wells where the percentage of clay was below 50%. The analysis of results showed that, assuming a business-as-usual management scenario, the impacts of CC on subsidence would be very significant for the case study. The mean increase of the maximum subsidence rates in the considered wells for the future horizon (2016–2045) and the RCP scenario 8.5 was 54%. In order to avoid undesirable consequences/risks as observed in other regions worldwide (Jakarta, Ho Chi Min City, and Bangkok, among others) where land subsidence is causing severe impacts—permanent inundation of land, aggravated flooding, changes in topographic gradients, rupture of the land surface, structural damage to buildings and infrastructures, and reduced capacity of aquifers to store water—some adaptation strategies should be applied to control and minimize the land subsidence caused by groundwater withdrawals.

Author Contributions: D.P.-V. and R.M.M. conceived and designed the research; P.E. analyzed the subsidence data; A.-J.C.-L. analyzed the data and conducted the experiments. All authors contributed to writing the manuscript. All authors have read and agreed to the published version of the manuscript.

Funding: This research was partially supported by the research projects SIGLO-AN (RTI2018-101397-B-I00) from the Spanish Ministry of Science, Innovation and Universities (Programa Estatal de I+D+I orientada a los Retos de la Sociedad) and the GeoE.171.008-TACTIC project from GeoERA organization funded by European Union's Horizon 2020 research and innovation program.

Acknowledgments: We would like to thank the Spain02 and CORDEX projects, the ENVISAT, Cosmo-SkyMed and Sentinel satellites, the Spanish Statistical Office, the Spanish official network for monitoring the quantitative state of groundwater and the Guadalquivir River Basin authority for the data provided for this study.

Conflicts of Interest: The authors declare no conflict of interest.

References

1. Abidin, H.Z.; Andreas, H.; Gumilar, I.; Fukuda, Y.; Pohan, Y.; Deguchi, T. Land subsidence of Jakarta (Indonesia) and its relation with urban development. *Nat. Hazards* **2011**, *59*, 1753. [CrossRef]
2. Lixin, Y.; Jie, W.; Chuanqing, S.; Guo, J.W.; Yanxiang, J.; Liu, B. Land Subsidence Disaster Survey and Its Economic Loss Assessment in Tianjin, China. *Nat. Hazards Rev.* **2010**, *11*, 35–41. [CrossRef]
3. Pacheco-Martínez, J.; Hernández-Marín, M.; Burbey, T.J.; González-Cervantes, N.; Ortiz, J.; Solís-Pinto, A. Land subsidence and ground failure associated to groundwater exploitation in the Aguascalientes Valley, México. *Eng. Geol.* **2013**, *164*, 172–186. [CrossRef]
4. Wang, G.Y.; Zhang, D.; Feng, J.S.; Chen, M.Z.; Shan, W.H. Land subsidence due to deep groundwater withdrawal in northern Yangtze river delta area. In *Engineering Geology for Society and Territory, Urban Geology, Sustainable Planning and Landscape Exploitation*; Springer: Cham, Switzerland, 2015; Volume 5. [CrossRef]
5. Ye, S.; Xue, Y.; Wu, J.; Yan, X.; Yu, J. Progression and mitigation of land subsidence in China. *Hydrogeol. J.* **2016**, *24*, 685–693. [CrossRef]
6. Faunt, C.C.; Sneed, M.; Traum, J.; Brandt, J.T. Water availability and land subsidence in the Central Valley, California, USA. *Hydrogeol. J.* **2016**, *24*, 675–684. [CrossRef]
7. De Luna, R.M.R.; Garnés, S.J.A.; Cabral, J.J.S.P.; Melo dos Santos, S. Groundwater overexploitation and soil subsidence monitoring in Recife plain (Brazil). *Nat. Hazards* **2017**, *86*, 1363. [CrossRef]
8. Erkens, G.; Bucx, T.; Dam, R.; de Lange, G.; Lambert, J. Sinking coastal cities. In *Prevention and Mitigation of Natural and Anthropogenic Hazards Due to Land Subsidence, Proceedings of the IAHS, Nagoya, Japan, 12 November 2015*; Daito, K., Galloway, D., Eds.; Copernicus Publications: Göttingen, Germany, 2015; Volume 372, pp. 189–198.
9. Galloway, D.L.; Burbey, T.J. Review: Regional land subsidence accompanying groundwater extraction. *Hydrogeol. J.* **2011**, *19*, 1459–1486. [CrossRef]
10. Galloway, D.L.; Erkens, G.; Kuniansky, E.; Rowland, J. Preface: Land subsidence processes. *Hydrogeol. J.* **2016**, *24*, 547–550. [CrossRef]
11. Tomás, R.; Romero, R.; Mulas, J.; Marturiá, J.; Mallorqui, J.; López-Sánchez, J.M.; Hererra, G.; Gutiérrez, F.; González, P.; Fernández, J.; et al. Radar interferometry techniques for the study of ground subsidence phenomena: A review of practical issues through cases in Spain. *Environ. Earth Sci.* **2014**, *71*, 163–181. [CrossRef]
12. Chaussard, E.; Wdowinski, S.; Cabral-Cano, E.; Amelung, F. Land subsidence in central Mexico detected by ALOS InSAR time-series. *Remote Sens. Environ.* **2014**, *140*, 94–106. [CrossRef]
13. Mahmud, M.U.; Yakubu, T.A.; Oluwafemi, O.; Sousa, J.J.; Ruiz-Armenteros, A.M.; Arroyo-Parras, J.G.; Bakoň, M.; Lazecky, M.; Perissin, D. Application of Multi-Temporal Interferometric Synthetic Aperture Radar (MT-InSAR) technique to Land Deformation Monitoring in Warri Metropolis, Delta State, Nigeria. *Procedia Comput. Sci.* **2016**, *100*, 1220–1227. [CrossRef]
14. Chen, M.; Tomás, R.; Li, Z.; Motagh, M.; Li, T.; Hu, L.; Gong, H.; Li, X.; Yu, J.; Gong, X. Imaging Land Subsidence Induced by Groundwater Extraction in Beijing (China) Using Satellite Radar Interferometry. *Remote Sens.* **2016**, *8*, 468. [CrossRef]
15. Mateos, R.M.; Ezquerro, P.; Luque, J.A.; Béjar-Pizarro, M.; Notti, D.; Azañón, J.M.; Montserrat, O.; Herrera, G.; Fernández-Chacón, F.; Peinado, T.; et al. Multiband PSInSAR and long-period monitoring of land subsidence in a strategic detrital aquifer (Vega de Granada, SE Spain): An approach to support management decisions. *J. Hydrol.* **2017**, *533*, 71–87. [CrossRef]
16. Meisina, C.; Zucca, F.; Notti, D.; Colombo, A.; Cicchi, A.; Savio, G.; Giannico, C.; Bianchi, M. Geological interpretation of PSInSAR Data at regional scale. *Sensors* **2008**, *8*, 7469–7492. [CrossRef] [PubMed]
17. Burbey, T.J.; Zhang, M. Inverse modeling using PSInSAR for improved calibration of hydraulic parameters and prediction of future subsidence for Las Vegas Valley, USA. In Proceedings of the International Association of Hydrological Sciences (IAHS '15), Nagoya, Japan, 12 November 2015; Volume 372, pp. 411–416.
18. Leake, S.A.; Galloway, D.L. *MODFLOW Ground-Water Model—User Guide to the Subsidence and Aquifer-System Compaction Package (SUB-WT) for Water-Table Aquifers*; Techniques and Methods; U.S. Geological Survey: Reston, VA, USA, 2007; p. 42.

19. Rahmati, O.; Falah, F.; Naghibi, S.; Biggs, T.; Soltani, M.; Deo, R.; Cerdà, A.; Mohammadi, F.; Tien Bui, D. Land subsidence modelling using tree-based machine learning algorithms. *Sci. Total Environ.* **2019**, *672*, 239–252. [CrossRef] [PubMed]
20. Li, J. A nonlinear elastic solution for 1-D subsidence due to aquifer storage and recovery applications. *Hydrogeol. J.* **2003**, *11*, 646–658. [CrossRef]
21. Ezquerro, P.; Guardiola-Albert, C.; Herrera, G.; Fernandez-Merodo, J.A.; Bejar, M.; Bonì, R. Groundwater and Subsidence Modeling Combining Geological and Multi-Satellite SAR Data over the Alto Guadalentín Aquifer (SE Spain). *Geofluids* **2017**, 1–17. [CrossRef]
22. IPCC. *Climate Change 2014: Impacts, Adaptation, and Vulnerability. Part A: Global and Sectoral Aspects*; Field, C.B., Barros, V.R., Dokken, D.J., Mach, K.J., Mastrandrea, M.D., Bilir, T.E., Chatterjee, M., Ebi, K.L., Estrada, Y.O., Genova, R.C., et al., Eds.; Contribution of working group II to the fifth assessment report of the intergovernmental panel on climate change; Cambridge University Press: Cambridge, UK; New York, NY, USA, 2014.
23. Dragoni, W.; Sukhija, B.S. Climate change and groundwater—A short review. In *Climate Change and Groundwater*; Dragoni, W., Sikhija, B.S., Eds.; Special Publications; Geological Society: London, UK, 2008; Volume 288, pp. 1–12.
24. Collados-Lara, A.J.; Pulido-Velazquez, D.; Pardo-Igúzquiza, E. An Integrated Statistical Method to Generate Potential Future Climate Scenarios to Analyse Droughts. *Water* **2018**, *10*, 1224. [CrossRef]
25. UN. *Guidance on Water y Adaptation to Climate Change*; ECE/MP.WAT/30; United Nations: Geneva, Switzerland, 2009.
26. Teng, J.; Chiew, F.; Vaze, J.; Marvanek, S.; Kirono, D. Estimation of Climate Change Impact on Mean Annual Runoff across Continental Australia Using Budyko and Fu Equations and Hydrological Models. *J. Hydrometeorol.* **2012**, *13*, 1094–1106. [CrossRef]
27. Verzano, K.; Bärlund, I.; Flörke, M.; Lehner, B.; Kynast, E.; Voß, F.; Alcamo, J. Modeling variable river flow velocity on continental scale: Current situation and climate change impacts in Europe. *J. Hydrol.* **2012**, *424*, 238–251. [CrossRef]
28. Pulido-Velazquez, D.; Collados-Lara, A.J.; Alcalá, F.J. Assessing impacts of future potential climate change scenarios on aquifer recharge in continental Spain. *J. Hydrol.* **2018**, *567*, 803–819. [CrossRef]
29. Barranco, L.M.; Álvarez-Rodríguez, J.; Olivera, F.; Potenciano, A.; Quintas, L.; Estrada, F. Assessment of the Expected Runoff Change in Spain Using Climate Simulations. *J. Hydrol. Eng.* **2014**, *19*, 1481–1490. [CrossRef]
30. Escriva-Bou, A.; Pulido-Velazquez, M.; Pulido-Velazquez, D. The Economic Value of Adaptive Strategies to Global Change for Water Management in Spain's Jucar Basin. *J. Water Resour. Plan. Manag.* **2017**, *143*, 5. [CrossRef]
31. Pulido-Velazquez, D.; Garrote, L.; Andreu, J.; Martin-Carrasco, F.J.; Iglesias, A. A methodology to diagnose the effect of climate change and to identify adaptive strategies to reduce its impacts in conjunctive-use systems at basin scale. *J. Hydrol.* **2011**, *405*, 110–122. [CrossRef]
32. Pulido-Velázquez, D.; García-Aróstegui, J.L.; Molina, J.L.; Pulido-Velázquez, M. Assessment of future groundwater recharge in semi-arid regions under climate change scenarios (Serral-Salinas aquifer, SE Spain). Could increased rainfall variability increase the recharge rate? *Hydrol. Process.* **2015**, *29*, 828–844. [CrossRef]
33. Hanson, R.; Flint, A.; Flint, L.; Faunt, C.; Schmid, W.; Dettinger, M.; Leake, S.; Cayan, R.D. Integrated simulation of consumptive use and land subsidence in the Central Valley, California, for the past and for a future subject to urbanization and climate change. In Proceedings of the Eighth International Symposium on Land Subsidence (EISOLS), Queretaro, Mexico, 17–22 October 2010; IAHS Publ.: Wallingford, UK, 2010; Volume 339, pp. 17–22.
34. Brouns, K.; Eikelboom, T.; Jansen, P.C.; Janssen, R.; Kwakernaak, C.; van den Akker, J.J.H.; Verhoeven, J.T.A. Spatial Analysis of Soil Subsidence in Peat Meadow Areas in Friesland in Relation to Land and Water Management, Climate Change, and Adaptation. *Environ. Manag.* **2014**, 55. [CrossRef]
35. Zhou, Y.; Li, W. A review of regional groundwater flow modeling. *Geosci. Front.* **2011**, *2*, 205–214. [CrossRef]
36. Skaugen, T.; Peerebom, I.O.; Nilsson, A. Use of a parsimonious rainfallrunoff model for predicting hydrological response in ungauged basins. *Hydrol. Process.* **2015**, *29*, 1999–2013. [CrossRef]
37. Tornqvist, T.E.; Wallace, D.J.; Storms, J.E.A.; Wallinga, J.; van Dam, R.L.; Blaauw, M.; Derksen, M.S.; Klerks, C.J.W.; Meijneken, C.; Snijders, E.M.A. Mississippi delta subsidence primarily caused by compaction of Holocene strata. *Nat. Geosci.* **2008**, *1*, 173–176. [CrossRef]

38. Parcharidis, I.; Kourkouli, P.; Karymbalis, E.; Foumelis, M.; Karathanassi, V. Time Series Synthetic Aperture Radar Interferometry for Ground Deformation Monitoring over a Small Scale Tectonically Active Deltaic Environment (Mornos, Central Greece). *J. Coast. Res.* **2013**, *29*, 325–338. [CrossRef]
39. Pulido-Velazquez, D.; Sahuquillo, A.; Andreu, J.; Pulido-Velazquez, M. A general methodology to simulate groundwater flow of unconfined aquifers with a reduced computational cost. *J. Hydrol.* **2007**, *338*, 42–56. [CrossRef]
40. Llopis-Albert, C.; Pulido-Velazquez, D. Using MODFLOW code to approach transient hydraulic head with a sharp-interface solution. *Hydrol. Process.* **2015**, *29*, 2052–2064. [CrossRef]
41. Kohfahl, C.; Sprenger, C.; Herrera, J.B.; Meyer, H.; Chacón, F.F.; Pekdeger, A. Recharge sources and hydrogeochemical evolution of groundwater in semiarid and karstic environments: A field study in the Granada Basin (Southern Spain). *Appl. Geochem.* **2008**, *23*, 846–862. [CrossRef]
42. Azañón, J.M.; Azor, A.; Booth-Rea, G.; Torcal, F. Small-scale faulting, topographic steps and seismic ruptures in the Alhambra (Granada, southeast Spain). *J. Quat. Sci.* **2004**, *19*, 219–227. [CrossRef]
43. Luque-Espinar, J.A.; Chica-Olmo, M.; Pardo-Igúzquiza, E.; García-Soldado, M.J. Influence of climatological cycles on hydraulic heads across a Spanish aquifer. *J. Hydrol.* **2008**, *354*, 33–52. [CrossRef]
44. Herrera, S.; Fernández, J.; Gutiérrez, J.M. Update of the Spain02 Gridded Observational Dataset for Euro-CORDEX evaluation: Assessing the Effect of the Interpolation Methodology. *Int. J. Climatol.* **2016**, *36*, 900–908. [CrossRef]
45. CORDEX PROJECT. The Coordinated Regional Climate Downscaling Experiment (CORDEX). Program Sponsored by World Climate Research Program (WCRP). 2013. Available online: https://www.wcrp-climate.org/news/wcrp-newsletter/wcrp-news-articles/1347-wcrp-spotlight-the-coordinated-regional-climate-downscaling-experiment-cordex (accessed on 11 January 2020).
46. Devanthéry, N.; Crosetto, M.; Monserrat, O.; Cuevas-González, M.; Crippa, B. An approach to persistent scatterer interferometry. *Remote Sens.* **2014**, *6*, 6662–6679. [CrossRef]
47. Barra, A.; Monserrat, O.; Mazzanti, P.; Esposito, C.; Crosetto, M.; Scarascia Mugnozza, G. First insights on the potential of Sentinel-1 for landslides detection. *Geomat. Nat. Hazards Risk* **2016**, *7*, 1874–1883. [CrossRef]
48. Hashmi, M.Z.; Shamseldin, A.Y.; Melville, B.W. Statistically downscaled probabilistic multi-model ensemble projections of precipitation change in a watershed. *Hydrol. Process.* **2013**, *27*, 1021–1032. [CrossRef]
49. Scott, C.A. The Water-Energy-Climate Nexus: Resources and Policy Outlook for Aquifers in Mexico. *Water Resour. Res.* **2011**, *47*, 1–18. [CrossRef]
50. Miller, M.M.; Shirzaei, M.; Argus, D. Aquifer Mechanical Properties and Decelerated Compaction in Tucson, Arizona. *J. Geophys. Res. Solid Earth* **2017**, *122*, 8402–8416. [CrossRef]